

REGULAR PAPER

A survey of human pilot models for study of Pilot-Induced Oscillation (PIO) in longitudinal aircraft motion

J.H. Bidinotto , H.C. Moura and J.P.C.A. Macedo

University of São Paulo, São Carlos School of Engineering, Department of Aeronautics Engineering, São Carlos – SP, Brazil,
E-mail: jhbidi@sc.usp.br

Received: 24 September 2020; **Revised:** 2 March 2021; **Accepted:** 26 August 2021

Keywords: PIO; pilot models; aircraft longitudinal motion; human survey

Abstract

Pilot-Induced Oscillation (PIO), although an old issue, still poses a significant threat to aviation safety. The introduction of new systems in modern aircraft modifies the human–machine interaction and makes it necessary for research to revisit the subject from time to time. Given the need of aircraft manufacturers to constantly perform PIO tests, this study analysed the feasibility of using three different computational pilot models (*Tustin*, *Crossover* and *Precision*) to simulate PIO conditions. Three aircraft models with different levels of propensity to PIO (*original*, *low propensity* and *high propensity*) were tested, as well as two pilot gain conditions (*normal* and *high*). Data were collected for a purely longitudinal synthetic task through simulations conducted in MATLAB®. PIO conditions were detected using a tuned PIO detection algorithm (ROVER). Data were analysed in terms of both whether the pilot models triggered a PIO condition and for how long the condition was sustained. The results indicated that the three pilot models only provoked PIO conditions when high gain inputs were applied. Additionally, *Crossover* was the only pilot model to trigger a PIO for the three aircraft models. There were also significant differences between the pilot models in the total PIO time, as the *Tustin* model typically sustained the oscillatory condition for longer.

Nomenclature

A	state matrix
A –PC	aircraft–pilot coupling
B	input matrix
C	output matrix
c	input vector
D	feedforward matrix
$e(s)$	error signal between the desired value and the actual aircraft
g	gravitational acceleration
I_y	moment of inertia about the y-axis
K_p	gain
LQR	linear quadratic regulator
m	mass of the aircraft
PIO	pilot-induced oscillation
q	pitch rate
ROVER	real-time oscillation verifier
T_L	general lead time constant of human pilot modelling function
T_I	general lag time constant of human pilot modelling function
$u(s)$	pilot control signal
Δu	longitudinal velocity variation
w	vertical velocity

\mathbf{x}	state vector
X, I, M	stability and control longitudinal derivatives
\mathbf{y}	linearised flight dynamics
$Y_c(s)$	transfer function for the aircraft behaviour
$Y_p(s)$	transfer function for human pilot action

Greek symbol

δ_e	elevator angle
$\Delta\theta$	pitch angle variation
ζ	damping coefficient
θ_0	initial pitch angle
τ, τ_e	time delay constant
ω_c	crossover frequency
ω_n	natural frequency

1.0 Introduction

Pilot-Induced Oscillation (PIO), also known as Aircraft–Pilot Coupling (A–PC), can be defined as “sustained or uncontrollable oscillations resulting from efforts of the pilot to control the aircraft” [1]. In other words, it is a coupling between the dynamics of a system (in this case, an aircraft) and the action of the pilot trying to control the oscillations but, instead of attenuating them, the controller aggravates the problem [2]. Although an old issue that has been studied since the 1960s [3], new PIO incidents, and even accidents, still occur in modern aircraft. The constant increase in performance and the introduction of new technologies foster research to revisit the topic from time to time [4]. The detection and suppression of PIO situations have been addressed by scientific researchers since the 1960s, and their results have shown that this phenomenon cannot be detected prior to its occurrence, although some algorithms propose real-time identification of the event, including the Real-time Oscillation Verifier (ROVER), which observes four parameters and their threshold values in order to characterise a PIO.

With the advancement of computational tools and the development of more reliable aircraft models, computational simulations have become a great ally in the analysis of PIO occurrences, as they are much cheaper and safer than carrying out in-flight test campaigns, which expose the aircraft to potential damage and endanger the test crew. Given that both the aircraft and the human pilot participate in a PIO, models of the vehicle dynamics and the human being are necessary for a representative simulation.

Several advances have been made towards high-fidelity physics-based aircraft models, which are now widely available, for example, through sets of control and stability derivatives in a state-space formulation. Computational pilot models have also benefited from recent major developments, especially the so-called *functional models*. However, to date, it is still unclear how these pilot models can be used to simulate PIO conditions.

To fill this gap, this study analysed the feasibility of using three different computational pilot models (*Tustin* [5], *Crossover* and *Precision* [6]) to simulate pitch PIO conditions. Tests were performed in MATLAB® for three aircraft models with different levels of propensity to PIO, as well as for two pilot gain conditions. A purely longitudinal synthetic task was used to induce potential PIOs, and a tuned real-time PIO detection algorithm (ROVER) was utilised to detect the condition.

The current paper is structured into the following main sections: Section 2 presents the modelling addressed for the PIO study, detailing the aircraft and pilot models, the synthetic task and the PIO detection algorithm, including some considerations about the flight commands; Section 3 details the data collection and estimation parameters required by the pilot functional models to perform the PIO computational simulations; Section 4 presents and discusses the findings. Finally, Section 5 provides concluding remarks. This work is part of a broader research project towards the study of PIO events [7,8].

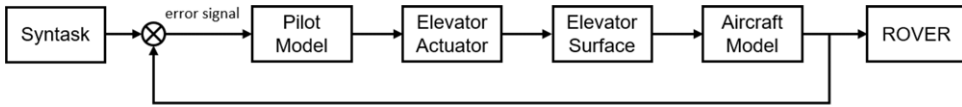


Figure 1. Diagram of the system used.

2.0 Modelling

In this manuscript, potential PIO conditions were assessed using the control arrangement shown in Fig. 1. It essentially consisted of a generic task to be performed (Syntask), a human pilot model, an aircraft model and a PIO detection algorithm (ROVER). Figure 1 also includes the elevator actuator and the elevator surface, representing the whole pitch flight control system. These are sources of delays and may affect the behaviour of the system in PIO [2,3,7-9], but in the current study, such delays were disregarded because they could compromise the information sought by the research.

The study focused on pitch PIO, thus only the longitudinal motion of the aircraft was considered and the pitch angle was chosen as the parameter to be controlled. That said, the error signal $e(s)$ shown in Fig. 1 accounted for the difference between the longitudinal reference attitude (the Syntask) and the actual pitch angle of the aircraft. Based on this signal, the pilot model actuated on the aircraft dynamics by deflecting the elevator (being the only possible input signal).

The behaviour of the human pilot is either represented by three different pilot models in the form of transfer functions proposed in the literature or by a real human, whereas the aircraft is modelled by the closed-loop configuration with a Linear Quadratic Regulator (LQR) controller. It is noteworthy that the actuators of the aircraft control surfaces have some limitations, thus their rate and position saturation were also modelled and incorporated into the vehicle dynamics model. The rate limit of the actuators was chosen to be 40°/s, and the position of the control surfaces was limited to deflect 30° for each side. Finally, the ROVER algorithm is utilised to identify in real time the occurrence of PIO [9].

The main blocks of the control arrangement of Fig. 1 are detailed in the remainder of this section.

2.1 Syntask

Syntask is a synthetic task consisting of a profile of attitudes (in our case, the pitch angle) to be carried out by either human or computational pilots. In this study, the Syntask was displayed on the artificial horizon by means of a movable red line (Fig. 2a). The line moved in accordance with the profile indicated in Fig. 2b. All simulations with the computational pilot models were performed using the same Syntask profile (Fig. 2b).

2.2 Aircraft model

A state-space approach according to Etkin and Reid (10) is selected to model the dynamics of the vehicle, in this case, a Boeing 747-100 in a cruise condition equivalent to an altitude of 40,000ft and Mach 0.8. Equation (1) describes the system via the state-space optics, in which the state vector \mathbf{x} represents the longitudinal velocity variation (Δu), vertical velocity (w), pitch rate (q) and pitch angle variation ($\Delta\theta$). It can thus be seen that only the longitudinal behaviour is considered, as the research focuses on pitch-axis PIO. For the same reason, the input vector of Equation (1), that is, \mathbf{c} , stands for the elevator angle (δ_e), while the output vector \mathbf{y} in the present research coincides with the state vector. Therefore, the output matrix \mathbf{C} is a 4×4 identity matrix, whilst the feedthrough matrix \mathbf{D} is a 4×1 null matrix. The throttle is considered to be constant.

$$\dot{\mathbf{x}} = \mathbf{Ax} + \mathbf{Bc} \tag{1}$$

$$\mathbf{y} = \mathbf{Cx} + \mathbf{Dc},$$

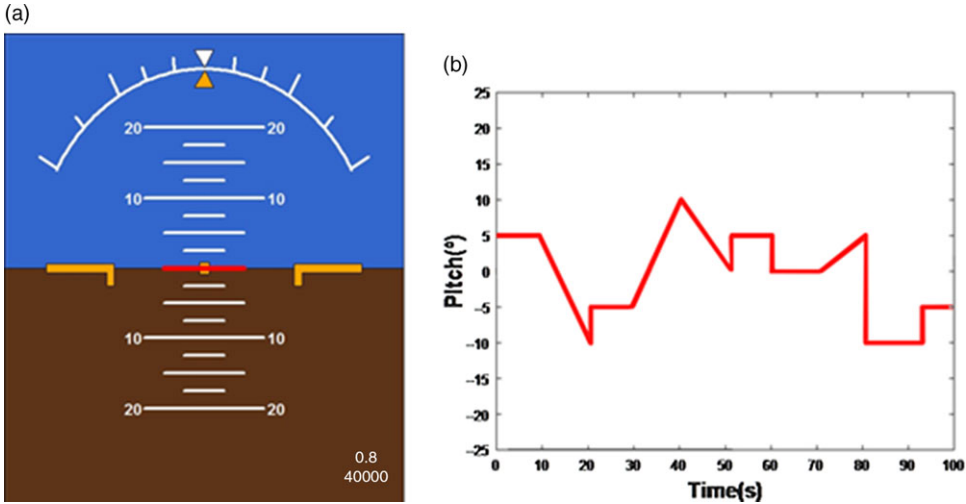


Figure 2. Synthetic task system [8].

which are presented as the Equations (2) and (3) when written in full mode

$$\begin{Bmatrix} \Delta \dot{u} \\ \dot{w} \\ \dot{q} \\ \Delta \dot{\theta} \end{Bmatrix} = \begin{pmatrix} \frac{X_u}{m} & \frac{X_w}{m} & 0 & -g \cos(\theta_0) \\ \frac{Z_u}{m-Z_{\dot{w}}} & \frac{Z_w}{m-Z_{\dot{w}}} & \frac{Z_q - m u_0}{m-Z_{\dot{w}}} & \frac{-mg \sin(\theta_0)}{m-Z_{\dot{w}}} \\ \frac{1}{I_y} \left[M_u + \frac{M_{\dot{w}} Z_u}{(m-Z_{\dot{w}})} \right] & \frac{1}{I_y} \left[M_w + \frac{M_{\dot{w}} Z_w}{(m-Z_{\dot{w}})} \right] & \frac{1}{I_y} \left[M_q + \frac{M_{\dot{w}} (Z_q + m u_0)}{(m-Z_{\dot{w}})} \right] & -\frac{M_{\dot{w}} mg \sin(\theta_0)}{I_y (m-Z_{\dot{w}})} \\ 0 & 0 & 1 & 0 \end{pmatrix} \begin{Bmatrix} \Delta u \\ w \\ q \\ \Delta \theta \end{Bmatrix} + \begin{pmatrix} \frac{X_{\delta_e}}{m} \\ \frac{X_{\delta_e}}{m-Z_{\dot{w}}} \\ \frac{M_{\delta_e}}{I_y} + \frac{M_{\dot{w}} Z_{\delta_e}}{I_y (m-Z_{\dot{w}})} \\ 0 \end{pmatrix} \delta_e, \quad (2)$$

$$\mathbf{y} = \begin{pmatrix} 1 & 0 & 0 & 0 \\ 0 & 1 & 0 & 0 \\ 0 & 0 & 1 & 0 \\ 0 & 0 & 0 & 1 \end{pmatrix} \begin{Bmatrix} \Delta u \\ w \\ q \\ \Delta \theta \end{Bmatrix} + \begin{pmatrix} 0 \\ 0 \\ 0 \\ 0 \end{pmatrix} \delta_e. \quad (3)$$

According to the assumption of decoupling between the longitudinal and lateral directional motions, Equations (2) and (3) apply to the motion relative to the axis in the wingspan direction (y). In these equations, m is the mass of the aircraft, g is the gravitational acceleration and I_y is the moment of inertia about the y -axis; the other terms are the longitudinal stability derivatives of the aircraft, detailed in Table 1.

A thorough investigation is conducted in the sense that three different sets of stability derivatives are analysed, as presented in Table 1. The first, model A, represents the original parameters for the mentioned flight condition [10], whilst models B and C [9], correspond to modified variables, with B being a model with lower propensity to PIO occurrence and C having a higher propensity. In Table 1, the derivatives omitted for models B and C mean that the original value was maintained.

2.3 ROVER algorithm

The ROVER algorithm seeks to detect PIO in real time by observing four parameters: (i) pitch rate magnitude, (ii) pitch rate frequency, (iii) pilot input amplitude and (iv) phase difference [11]. When

Table 1. The stability and control derivative of the models [9,10]

Stability Derivatives	Aircraft Model		
	Original (Model A)	Low propensity (Model B)	High propensity (Model C)
$X_{\dot{u}}$	-1.982×10^3	–	–
X_w	$+4.025 \times 10^3$	–	–
$Z_{\dot{u}}$	-2.595×10^4	–	–
Z_w	-9.030×10^4	$+9.030 \times 10^3$	–
Z_q	-4.524×10^5	$+1.610 \times 10^8$	–
Z_w^*	$+1.909 \times 10^3$	–	–
$M_{\dot{u}}$	$+1.593 \times 10^4$	–	–
M_w	-1.563×10^5	–	–
M_q	-1.521×10^7	–	$+1.171 \times 10^7$
M_w^*	-1.702×10^4	–	-8.510×10^4
X_{δ_e}	-1.653×10^1	–	–
Z_{δ_e}	-1.579×10^6	$+6.318 \times 10^7$	-3.257×10^8
M_{δ_e}	-5.204×10^7	-5.204×10^8	–

Table 2. ROVER parameters [11,12]

Parameter	Threshold value
Pitch rate magnitude	$\geq 8^\circ/s$
Pitch rate frequency	0.85–10rad/s
Pilot command	≥ 1.0 (peak to peak)
Phase difference	$\geq 40^\circ$

all these parameters simultaneously reach pre-established threshold values, the algorithm flags that the system is in PIO.

These parameter values were chosen according to Liu [12] and have been previously tested in other works from the same authors [7–9]. In these trials, some human pilots were subjected to similar conditions and their subjective opinion corroborated the use of the values presented in Table 2.

2.4 Pilot models

Three mathematical pilot models were used in this study. Although differing slightly, they all seek to mathematically represent the control action of a human pilot by means of a transfer function $Y_p(s)$ modelling the pilot control signal $u(s)$ for the error signal $e(s)$. The three models together with their transfer functions are described below.

2.4.1 Tustin model

Tustin [5] proposed the transfer function presented herein as Equation (4) to model the human pilot control action. In this model, the pilot’s control behaviour, level of experience and neuromuscular limitations are taken into account. These parameters are respectively represented in Equation (4) by the gain K_p , the time constant of anticipation T_L and the time delay constant τ .

$$Y_p = \frac{u(s)}{e(s)} = \frac{K_p(1 + T_L s)e^{-\tau s}}{s} \tag{4}$$

2.4.2 Crossover model

According to McRuer [6], human pilots adapt their control actions depending on how they perceive the dynamic condition of the controlled vehicle, thus that author proposed an open-loop transfer function for the pilot–vehicle system as presented in Equation (5).

$$Y_p Y_c = \frac{\omega_c e^{-\tau_e s}}{s}. \quad (5)$$

In this model, $Y_c(s)$ and $Y_p(s)$ represent the individual transfer functions of the vehicle and pilot, respectively, whereas ω_c is the so-called *crossover frequency* and τ_e is a total time delay constant modelling the time elapsed between the instant when a change in the system behaviour is identified by the human body and the moment the aircraft changes its attitude as a consequence of an action performed by the crew member.

Based on the mentioned pilot–vehicle system model, McRuer further explored the pilot behaviour and introduced a transfer function solely describing the human being as expressed in Equation (6). The presence of a time delay constant (T_I) suggests the adoption of this model when the response of a controlled plant is dominated by a second-order transfer function, which serves well the aircraft modes of phugoid, short-period and Dutch roll. Additionally, K_p stands for the gain of the pilot, and τ serves as their response time delay.

$$Y_p = \frac{u(s)}{e(s)} = \frac{K_p e^{-\tau s}}{T_I s + 1}. \quad (6)$$

2.4.3 Precision model

Likewise developed by McRuer [6], the precision model expands the crossover model to take into account the human neuromuscular actuation system and an anticipation component for the pilot's control action. The general form of its describing function is defined in Equation (7). In addition to the pilot gain K_p , time delay τ and general lag time constant T_I also considered in the crossover model, Equation (7) introduces the lead time constant T_L towards the lead-lag pilot control actuation, as well as the term in parentheses to account for the neuromuscular system. Regarding the latter, ω_n and ζ respectively represent the natural frequency and damping ratio of the pilot's neuromuscular system.

$$Y_p = K_p e^{-\tau s} \frac{T_L s + 1}{T_I s + 1} \left(\frac{1}{\frac{s^2}{\omega_n^2} + \frac{2\zeta}{\omega_n} s + 1} \right). \quad (7)$$

To utilise the models presented above, the parameters of each transfer function were obtained from experimental data gathered from human pilot trials. Thus, a model estimation methodology was applied, as detailed in the next section.

3.0 Model estimation

Human pilot trials are conducted to estimate the variables required by the pilot models. For this purpose, three volunteer pilots, identified as pilot 1, pilot 2 and pilot 3, were asked to fly the Boeing 747 model in the above-detailed cruise situation (Section 2.2). In these tests, the system shown in Fig. 1 still applies, except for the pilot model which is substituted by the human pilot, and the ROVER system, which in this case is not utilised.

The trials consist of the generation of a synthetic task in the form of a step from 0° to 10° (or 10° to 0°).¹ with respect to the artificial horizon (Fig. 2a). The pilots are then required to capture the angle using a commercial joystick with a 40Hz acquisition rate.

In addition, for the characterisation of a PIO condition, the pilot must apply the command in an aggressive manner [13], simulating an emergency situation. This way, both conditions are simulated:

¹As the dynamics of the aircraft is different when applying positive and negative commands, both tests were performed.

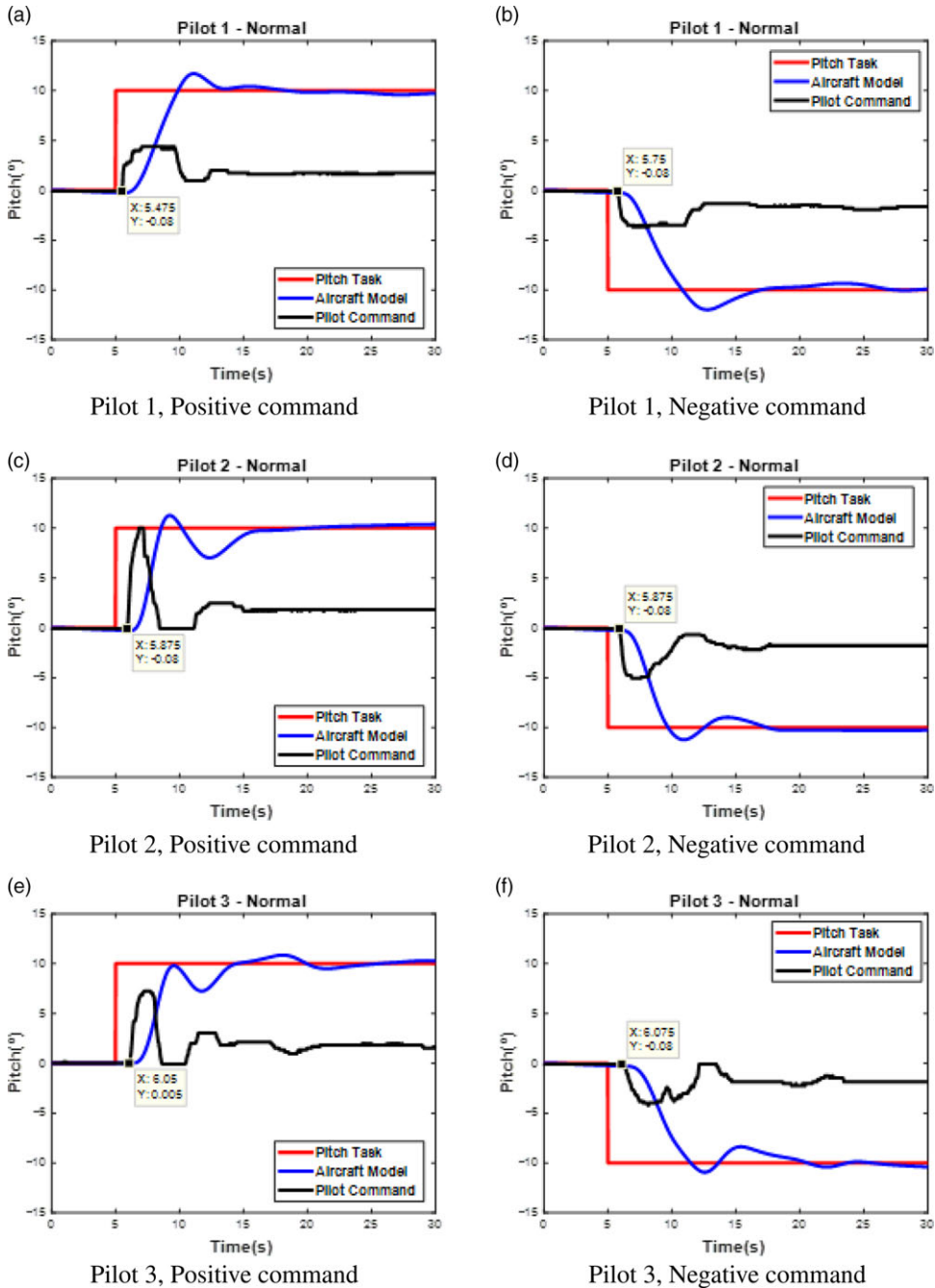


Figure 3. Pilot model estimation: Syntask, aircraft pitch angle and pilot input for the normal gain condition.

slow application (called *normal gain condition*) and fast application (called *high gain condition*). Hereinafter, these modes are also named *susceptibility conditions*.

Figures 3 and 4 present the results obtained for the three test pilots performing the task just described. In both cases, the *Pitch Task* curve (red) represents the synthetic task that the pilot should follow, while

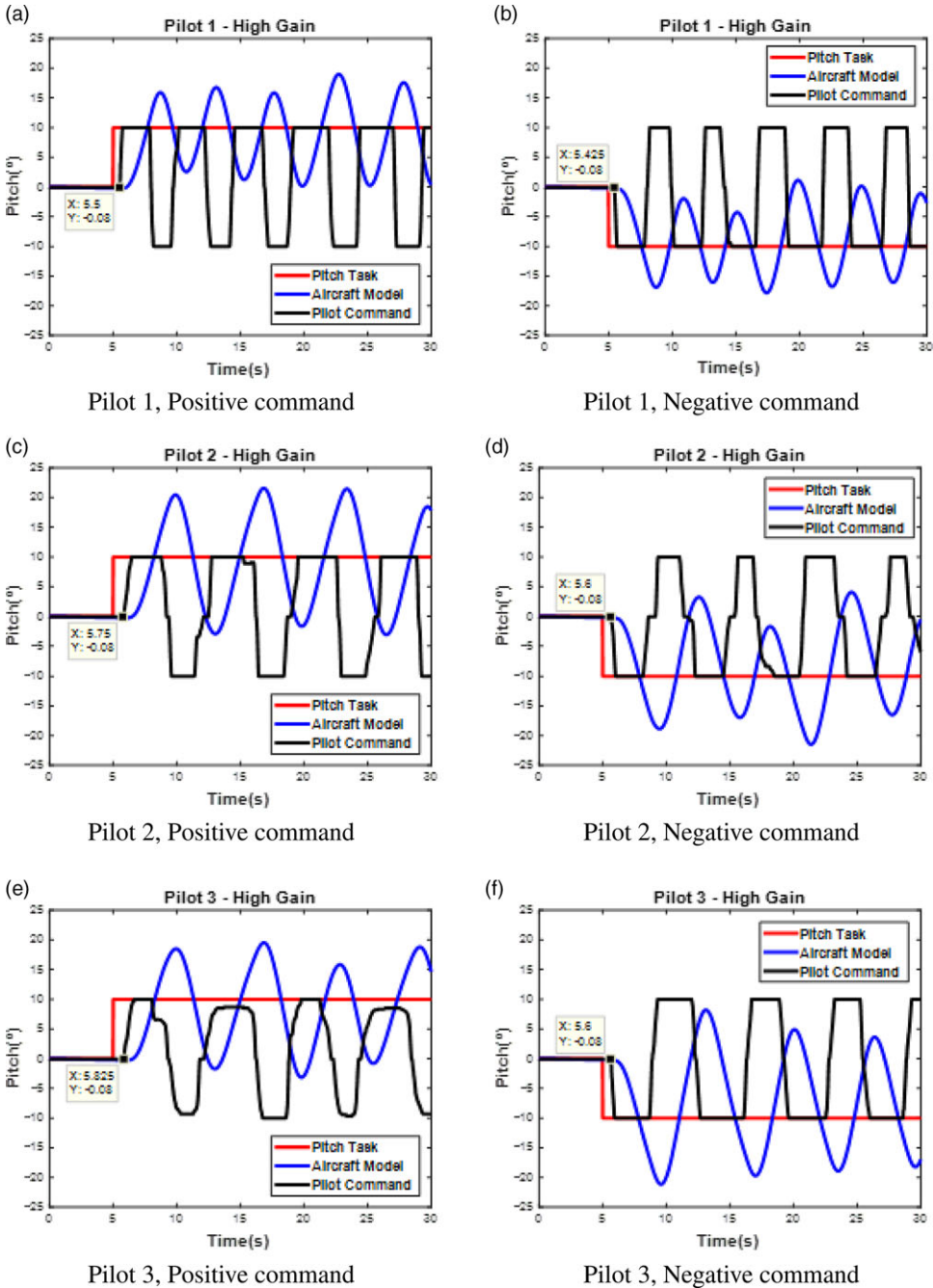


Figure 4. Pilot model estimation: Syntask, aircraft pitch angle and pilot input for the high gain condition.

the *Pilot Command* contour (black) shows the angle applied on the joystick by the test pilot, and finally, the curve labelled *Model Angle* (blue) is the attitude of the aircraft model following the command application. Figure 3 applies to the normal gain condition, whilst Fig. 4 refers to the high gain situation.

Table 3. Pilot model estimation: parameters for the normal gain condition

Pilot Model	Normal gain condition					
	K_p	T_L	T_I	ζ	ω_n	τ
Tustin	0.3715	5.5328	1×10^{-6}	–	–	0.85
Crossover	2.8820	–	0.2334	–	–	0.85
Precision	4.9475	6.5253	10	0.6460	18.1217	0.85

Table 4. Pilot model estimation: parameters for the high gain condition

Pilot Model	High gain condition					
	K_p	T_L	T_I	ζ	ω_n	τ
Tustin	1.0423	6.0390	1×10^{-6}	–	–	0.6167
Crossover	6.4706	–	0.1562	–	–	0.6167
Precision	5.9640	1.0095	0.8875	0.8	22.2916	0.6167

Table 5. Pilot model estimation: Z-domain transfer functions

Pilot Model	Susceptibility condition	
	Normal	High gain
Tustin	$Y_p = \frac{z^{-34}(1.989z - 1.979)}{z - 1}$	$Y_p = \frac{z^{-25}(6.303z - 6.277)}{z - 1}$
Crossover	$Y_p = \frac{z^{-34}(0.2928)}{z - 0.8984}$	$Y_p = \frac{z^{-25}(0.3348z + 0.221)}{z - 0.8521}$
Precision	$Y_p = \frac{z^{-34}(0.208z^2 - 0.04705z - 0.2218)}{z^3 - 2.402z^2 + 1.958z - 0.5555}$	$Y_p = \frac{z^{-25}(0.1051z^3 + 0.915z^2 - 0.7586z - 0.2282)}{z^3 - 2.182z^2 + 1.586z - 0.3986}$

From the data presented in Figs. 3 and 4, the parameters of interest for the three pilot models were extracted, for both the normal and high gain conditions, as presented in Table 3 and 4, respectively. To accomplish this task, the MATLAB® system identification toolbox was used, although due to limitations of the mentioned toolbox in identifying the real value of the pilot time delay, the pole of Tustin’s model, originally at the origin, was dislocated, resulting in the transfer function described in Equation (8)

$$Y_p = \frac{K_p(T_L s + 1)}{(T_I s + 1)} e^{-\tau s} \tag{8}$$

Finally, Table 5 provides the transfer functions for the three pilot models according to the gain condition. Entries in Table 5 are in the Z-domain (discrete-time), i.e.,

$$Y_p = \frac{u(z)}{e(z)} \tag{9}$$

4.0 Results

To investigate the PIO phenomenon, a series of mathematical simulations were conducted with the Boeing 747-100 in cruise condition. Referring to Fig. 1, Syntask corresponds to a given imposed task to be performed, whereas pilot model stands for the derived pilot functional models (Section 3, Table 5) in both normal and high gain conditions; furthermore, the *aircraft model* is substituted by the three vehicle models detailed in Table 1. Finally, the ROVER algorithm, as discussed in Sect. 2.3, is utilised to indicate the occurrence (or not) of PIO.

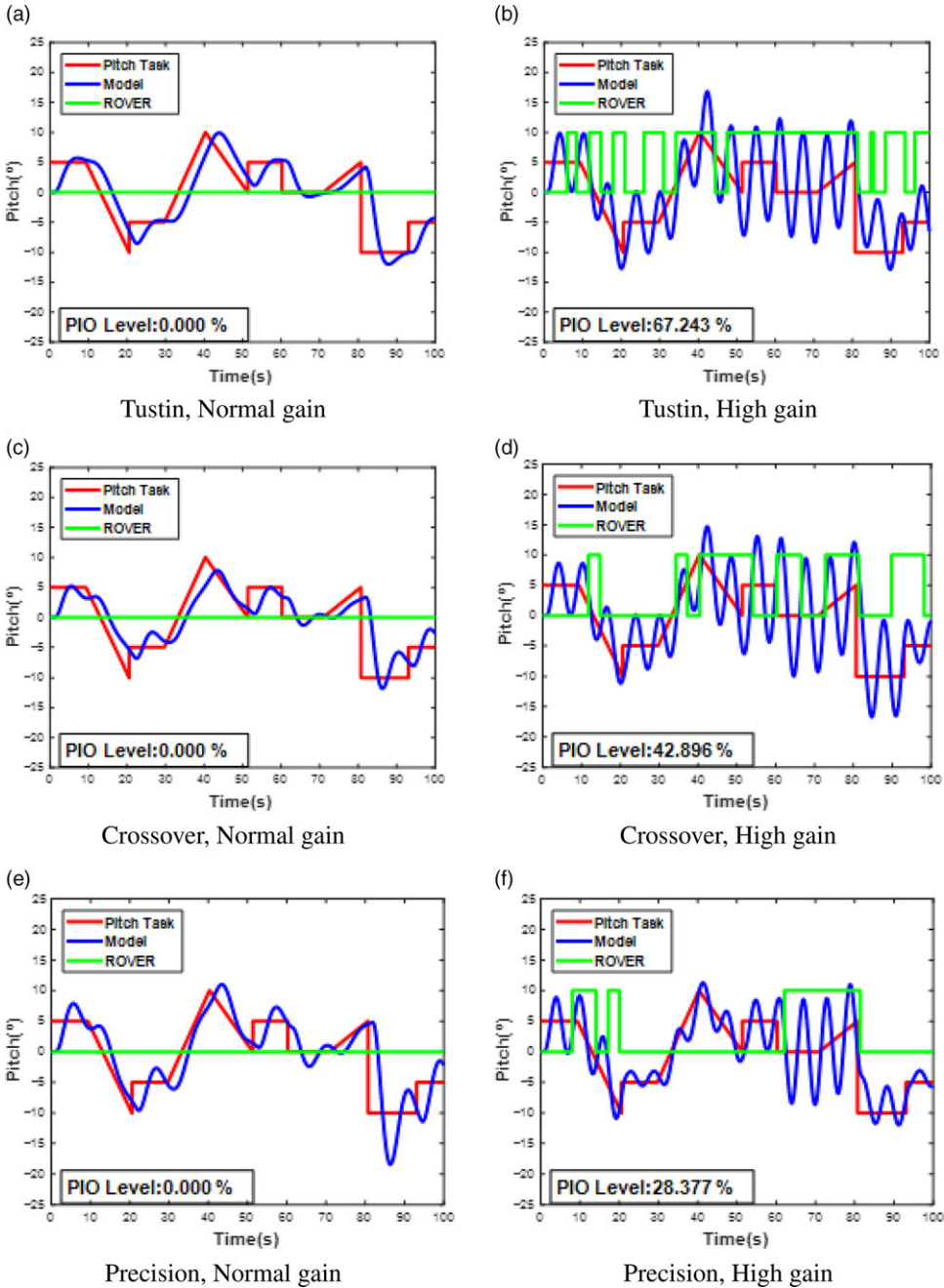


Figure 5. Syntask, Aircraft pitch angle and ROVER for all pilot models and gain conditions: original aircraft model (A).

The results are presented in Figs 5, 6 and 7. All of them present the control responses for the three pilot models (Tustin, Crossover and Precision) and susceptibility conditions (normal and high gain), although Fig. 5 refers to the original aircraft model (model A), whilst Figs. 6 and 7 correspond to the aircraft dataset with low (model B) and high (model C) propensity for PIO, respectively.

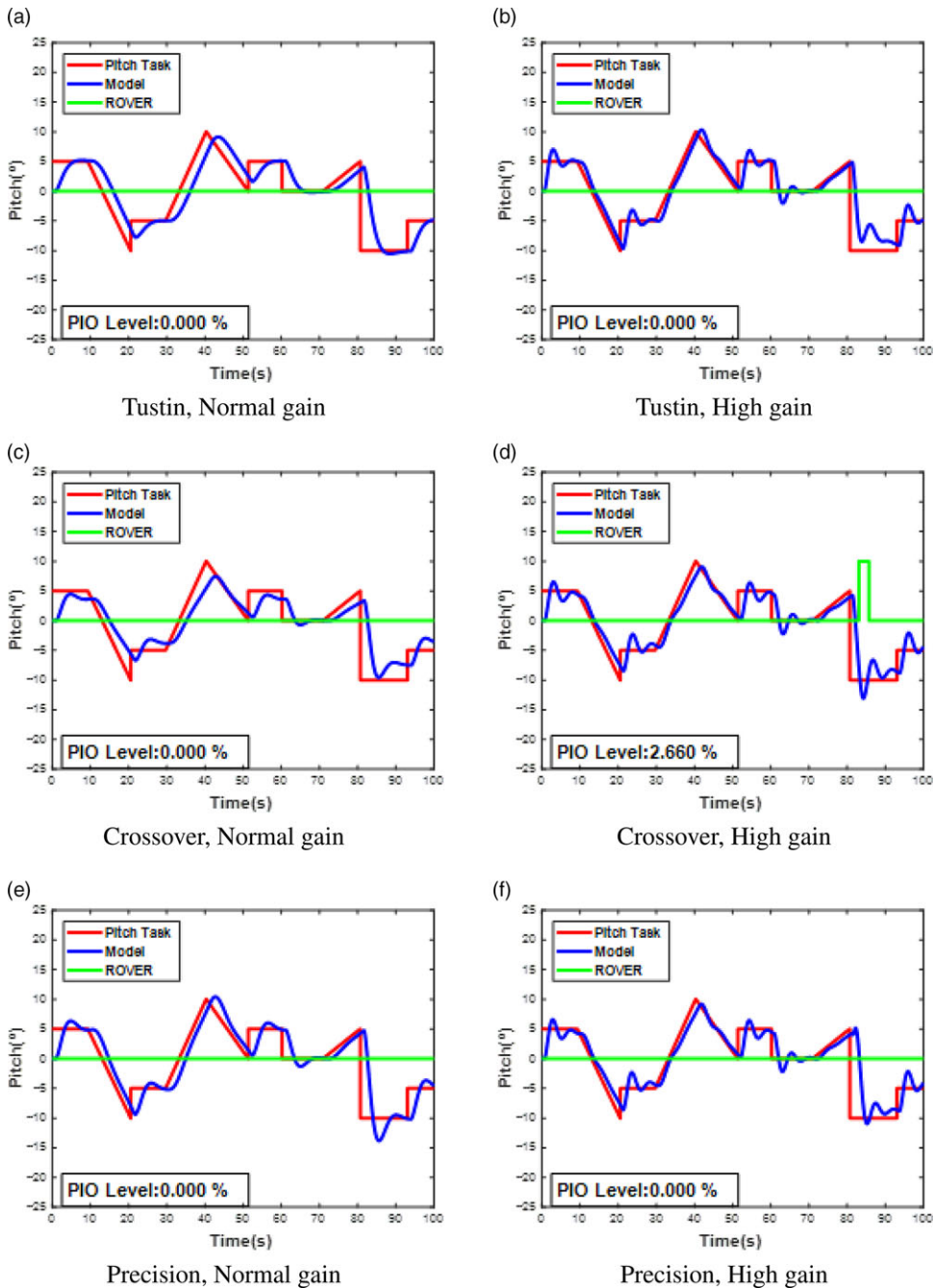


Figure 6. Syntask, Aircraft pitch angle and ROVER for all pilot models and gain conditions: low propensity model (B).

Additionally, in each figure, the *Pitch Task* (red) curve represents the synthetic task proposed to the virtual pilot, the *Model contour* (blue) shows the response of the pilot-controlled aircraft model and the *ROVER* curve (green) indicates the PIO condition based on the detection subroutine. In more detail, when the *ROVER* curve is zero, the pilot–aircraft set lies outside the PIO condition, while on the other

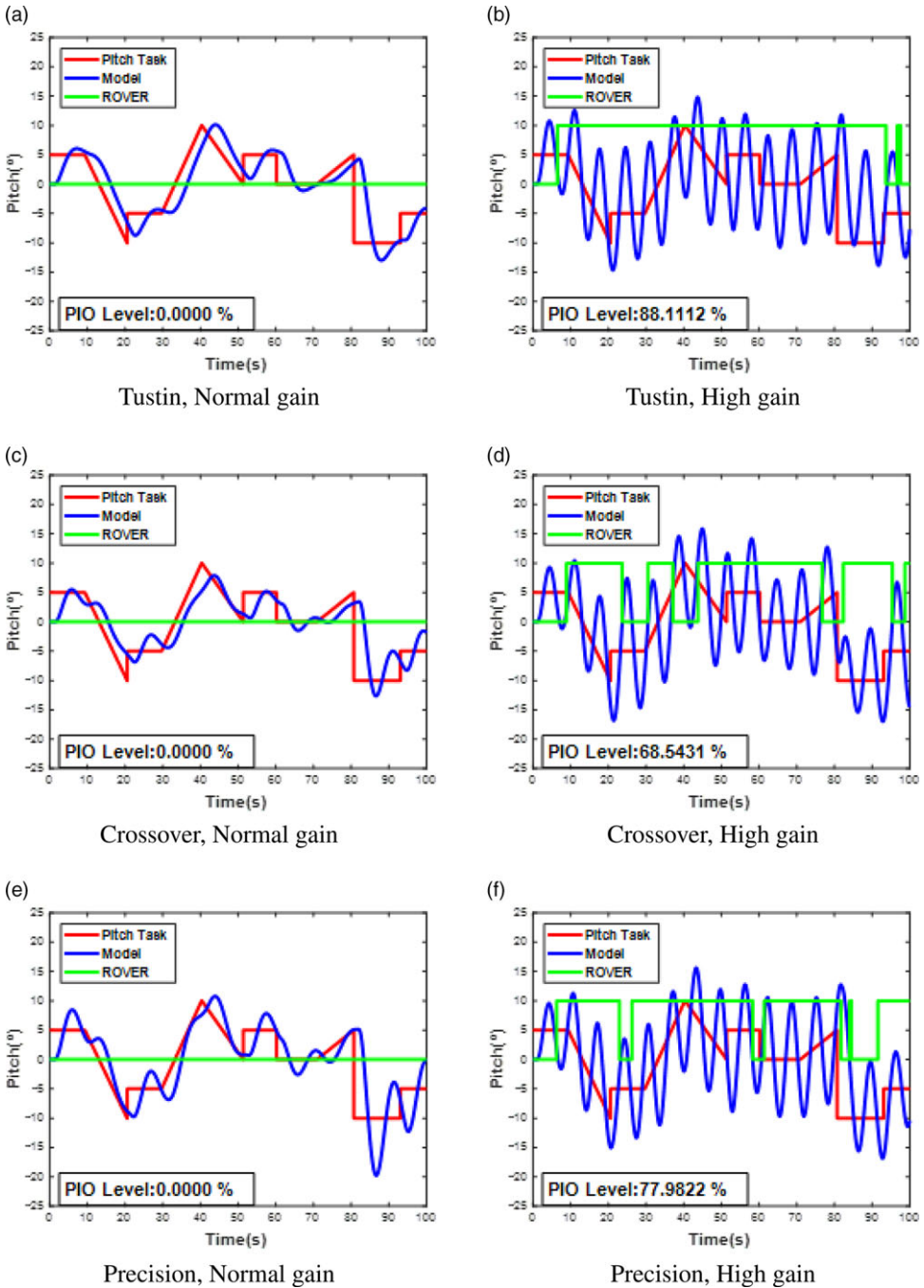


Figure 7. Syntask, Aircraft pitch angle and ROVER for all pilot models and gain conditions: high propensity model (B).

hand, when it assumes non-zero values (in this case chosen to be 10 in order to be better visualised in the figures), it means that the set is coupled, i.e., in a PIO condition.

Moreover, Fig. 5, 6 and 7 also present the variable *PIO Level*, that is, the percentage of time for which the ROVER curve is in 10 (non-null). As the subroutine serves for the detection of a PIO situation, it is

possible to infer that, the higher the *PIO Level*, the more susceptible to the phenomenon the pilot–aircraft system will be.

5.0 Conclusions

In the light of the collected results, it is possible to state that the proposed system architecture, as presented in Fig. 1, is effective for simulating the high gain condition, with both human and virtual pilots. Since the three pilot models were successfully applied in the simulations, it can be concluded that the methodology for estimating their transfer function parameters is adequate; moreover, as the ROVER subroutine identified the coupling between the aircraft and pilot, it can be concluded that the algorithm is valid for detecting PIO.

Based on theoretical literature, the high gain manoeuvring condition was expected to show a greater tendency to PIO when compared with the low-gain applications, which is indeed confirmed by the PIO level observations in Fig. 5, 6 and 7. Additionally, independently of the pilot model adopted, the aircraft models with low (B) and high (C) propensity for PIO proved to be in accordance with theoretical expectations, as the PIO level of these plants is considerably lower and higher, respectively, in comparison with the original aircraft dynamics. These observations are valid for the high gain command application condition.

For the low propensity aircraft model (B), only the Crossover pilot activated the ROVER algorithm (Fig. 6d). In comparison with the response obtained for the other virtual pilots, the mentioned model presents the greatest residual oscillation about the pitch task, which triggers the ROVER, confirming the sensitivity of the detection algorithm.

However, in this sense, for the high propensity aircraft model (C), the virtual pilot proposed by Tustin showed greater susceptibility to sustaining oscillations with the aircraft, being a more conservative option when studying pilot–aircraft coupling behaviour without the application of any type of control. On the other hand, for the original aircraft model (A), the virtual Crossover pilot model had a greater tendency to PIO when compared with the Precision model, whereas for the high propensity (C) model, the opposite is observed, with the Precision virtual pilot having a slightly greater tendency than the Crossover pilot representation.

In future research addressing PIO, it is recommended to identify the threshold values of the stability derivatives for cases with greater propensity for this phenomenon. Also, a project is already underway with the aim of deeper characterisation of the loss of control in flight phenomenon, which also includes the PIO problem based on a parametric analysis of pilot inputs and aircraft behaviour in both longitudinal and lateral axes.

In the near future, the authors aim to develop a tool that could detect and suppress the PIO condition in real time, to avoid future accidents caused by this phenomenon.

Acknowledgements. This work was supported by FAPESP (grant no. 2016/16808-5) and CNPq scholarship.

References

1. Department of Defense Interface Standard *Mil Standard, MIL1797A: Flying Qualities of Piloted Airplanes*, Washington D.C., 1995.
2. Wang, C., Santone, M. and Cao C. Pilot-induced oscillation suppression by using L1 adaptive control, *J Control Sci Eng*, May 2012, 2012, (1), pp 1–7.
3. Ashkenas, I. Pilot-induced oscillations: Their cause and analysis, *Tech. Report, DTIC Document*, 1964.
4. Toader, A. and Ursu, I. Pilot modeling based on time-delay synthesis, *Proc Inst Mech Eng G J Aerosp Eng*, March 2013, **228**, (5), pp 740–754.
5. Tustin, A. The nature of the operators response in manual control, and its implications for controller design, *J Inst Electr Eng - Part IIA: Automat Regulat Servo Mech*, May 1947, **94**, (2), pp 190–206.
6. McRuer, D.T. and Krendel, E. Mathematical models of human pilot behavior, AGARDograph, January 1974, n.o 188.
7. Moura, H.C., Bidinotto, J.H. and Belo, E.M. Pilot induced oscillations adaptive suppression in fly-by-wire systems, *World Acad Sci Eng Technol*, September 2018, **12**, (9), pp 870–876.

8. Moura, H.C. Supressão adaptativa de PIO em sistemas FBW, M.Sc. Dissertation - University of São Paulo (in portuguese), February 2018.
9. Moura, H.C., Alegre, G.S.P., Bidinotto, J.H. and Belo, E.M. PIO susceptibility in fly-by-wire systems, ICAS Proc 2018, September 2018.
10. Etkin, B. and Reid, L. *Dynamics of Flight – Stability and Control* - 3rd ed., 1996, John Willey and Sons.
11. Mitchell, D.G., Arencibia, J. and Munoz, S. Real-time detection of pilot-induced oscillations, *AIAA Atmospheric Flight Mechanics Conference and Exhibit*, August 2004, Providence, Rhode Island.
12. Liu, Q. Pilot-induced oscillation detection and mitigation, *M.Sc. Dissertation - Cranfield University*, December 2012.
13. Mitchell, D.G. and Klyde, D.H. Identifying a PIO – new techniques applied to an old problem, *J Guid Control Dyn*, January 2008, **31**, (1), pp 215–224.